Journal of Macromolecular Science, Part A
Publication details, including instructions for authors and subscription information:
http://www.informaworld.com/smpp/title~content=t713597274

Preparation and Characteration of UV-cured EA/MMT Nanocomposites Via *In-Situ* Polymerization

Guoliang Wu[a]; Guangpeng Liu[a]; Yangling Zang[a]; Yanbing Lu[a]; Yuanqin Xiong[a]; Weijian Xu[a]
[a] Institute of Polymer Science and Engineering, College of Chemistry and Chemical Engineering, Hunan University, Changsha, China

Online publication date: 09 June 2010

To cite this Article Wu, Guoliang , Liu, Guangpeng , Zang, Yangling , Lu, Yanbing , Xiong, Yuanqin and Xu, Weijian(2010) 'Preparation and Characteration of UV-cured EA/MMT Nanocomposites Via *In-Situ* Polymerization', Journal of Macromolecular Science, Part A, 47: 7, 647 — 654
To link to this Article: DOI: 10.1080/10601325.2010.483355
URL: http://dx.doi.org/10.1080/10601325.2010.483355

Journal of Macromolecular Science, Part A: Pure and Applied Chemistry (2010) **47**, 647–654

ISSN: 1060-1325 print / 1520-5738 online
DOI: 10.1080/10601325.2010.483355

Taylor & Francis
Taylor & Francis Group

Preparation and Characteration of UV-cured EA/MMT Nanocomposites Via *In-Situ* Polymerization

GUOLIANG WU, GUANGPENG LIU, YANGLING ZANG, YANBING LU, YUANQIN XIONG and WEIJIAN XU*

Institute of Polymer Science and Engineering, College of Chemistry and Chemical Engineering, Hunan University, Changsha, China

Received, Accepted January 2010

A long-chain surfactant, enzoylbenzyl-N,N-dimethyl-N-octadecylammonium bromide (BDOB) with a benzophenone group, was synthesized to modify the montmorillonites (MMT) for the preparation of nanocomposites via photo-induced polymerization. The BDOB-modified MMT was characterized by the fourier transform infrared spectrometer (FTIR), thermal gravimetric analyzer (TGA) and X-ray diffraction (XRD), and the results of XRD indicated that the intercalated structures of BDOB-modified MMT was obtained. The conversion of the bisphenol A epoxy diacrylate (EA) was quantified by the FTIR, and the results indicated that conversion increased with an increase in the amount of BDOB-modified MMT. The morphologies of the UV-cured EA/MMT nanocomposites prepared from this organically modified MMT were studied by means of XRD and TEM, and the results showed that all the samples contained an intercalated structure with partial exfoliated structure. The results of TGA and mechanical properties also indicated that the thermal and mechanical properties of UV-cured nanocomposites were significantly enhanced due to the presence of the long chain surfactant organically modified MMT.

Keywords: UV-cured nanocomposites, organically-modified MMT, *in-situ* polymerization, thermal and mechanical properties

1 Introduction

UV-curing technology offers a number of advantages, namely, ultrafast curing, ambient temperature operations, spatial and temporal control of the process, and a wide range of mechanical properties of the highly crosslinked polymer formed (1). It has been used in various areas of application, especially in the electronic industry due to its high efficiency, environmental friendliness and energy saving (2, 3). However, in some of the cases such as printed circuits, patterning (video disk), sealants (encapsulation) and conformal coatings, it is required to prepare a polymer film with higher glass transition temperature, enhanced barrier properties, low shrinkage, excellent mechanical properties and high thermal stability. Fortunately, the requirements could be satisfied with the application of clay nanotechnology. We know that numerous polymer properties, including those mentioned above, could be greatly enhanced even at a low loading of clays (4–7). Therefore, it is not surprising that UV-curable clay nanocomposites, which take advantage of both UV-curing and nanotechnology, have attracted so much attention in recent years since Zahouily et al. (8) first reported their preparation of UV curable polymer-clay nanocomposites.

In general, MMT is organically modified by the organic quaternary alkylammonium salts with long chains. The organic cations can reduce the surface energy of silicate layers and enhance the miscibility between the silicate layers and the polymer matrix, and the distance between the layers is enlarged (9, 10). The resulting structure allows clay to accommodate polymer chains and form polymer/clay nanocomposites (11, 12). Surfactants with reactive groups such as an acrylic group and a styrene group were employed to modify clays in order to improve the compatibility between the clay and the polymer matrix through the C=C double bonds participating in the following polymerization. A number of authors have reported improvements in physical properties with the inclusion of the typical alkyl ammounium modified nanoclays generally without significant changes to the polymerization kinetics of the acrylate or methacrylate itself (13, 14). Uhl et al. (15, 16) first proposed a method of using a novel benzophenone surfactant with acrylate functional groups to modify clays. Experimental results indicated that the UV-cured urethane acrylate/MMT nanocomposites prepared from this novel

*Address correspondence to: W. J. Xu, Institute of Polymer Science and Engineering, College of Chemistry and Chemical Engineering, Hunan University, Changsha 410082, China. Tel: +86-731-88821549; Fax: +86-731-88821549; E-mail: weijianxu_59@163.com

organically modified clay possessed intercalated or exfoliated structures. Keller et al. (17) described a method in which reactive acrylate-modified nanoclays were dispersed in the UV-cured urethane-acrylate, and the tensile strength and the elongation at break of UV-cured nanocomposites were greatly improved compared with the microcomposite containing the un-exfoliated clay filler. To expand the research on the compatibility between the clays and the polymer matrix, Yebassa et al. (18) studied the effect of the inclusion of a non-reactive and reactive modified clay in a thermally cured vinyl ester matrix and found that ion exchange of the reactive onium salt ω-undecylenyl amine hydrochloride and the non-reactive onium ion (undecyl amine hydrochloride) increased the gallery spacing to 0.42 and 0.41 nm, respectively. When these clays were dispersed in a vinyl ester resin using processing aids, such as ultrasonics, the reactive modified clay appeared to produce the highest degree of exfoliation as observed by using TEM. Wang et al. (19) reported an unusual geometrical surfactant with a reactive methacrylic group, GME-N-C_{10}, to effectively extend the lamellar spacing of clays in the preparation of organically modified clays. In our laboratory's previous study (20), a bifunctional reactive surfactant containing a polymerizable methacrylate group and a benzophenone group, [2-(methacryloyloxy)ethyl](4-benzoylbenzyl)dimethylammonium bromide (MDAB), was synthesized to modify montmorillonite (MMT) for the preparation of nanocomposites via photoinduced polymerization.

From the point of view above, however, little research was reported about an anchored polymeriable cationic photo-initiator-modified MMT used as the only photo-initiator for preparing the UV-cured EA/MMT nanocomposites. Therefore, in this study, we prepared UV-cured EA/MMT nanocomposites using a long-chain surfactant organically modified MMT as the only initiator via *in situ* polymerization, and further studied the effect of organically-modified MMT content on photopolymerization, the thermal stability and mechanical properties of the UV-cured EA/MMT nanocomposites, and the compatibility of the clays with polymer matrix.

2 Experimental

2.1 Materials

Bisphenol A epoxy diacrylate (EA, $M_n = 1200$), purchased from Sartomer Co. (Exton, PA), was used as telechelic oligomer. The reactive diluent, tripropyleneglycol diacrylate (TPGDA), was provided by UCB Co (Shanghai, China). The structures of EA and TPGDA were shown in Scheme 1. The pristine sodium montmorillonite (Na-MMT) was provided by Zhejiang Fenghong Clay Chemicals Co., Ltd. [cationic exchange capacity (CEC) = 90 meq/100 g]. Octadecyl dimethyl amine was purchased from Sinopharm Chemical Reagent Co., Ltd. (Beijing, China). 4-bromomethyl benzophenone was purchased from Alfa Aesar and used without further purification.

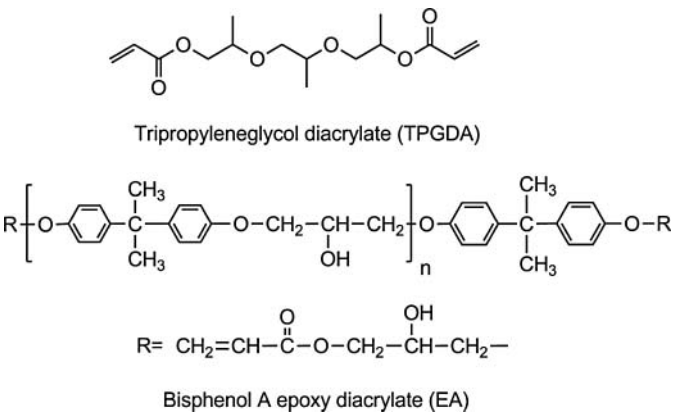

Sch. 1. Chemical structure of the components of UV-curable resins.

2.2 Synthesis of Benzoylbenzyl-N,N-Dimethyl-N-Octadecylammonium Bromide (BDOB)

The theoretical molecular structure of the resulting BDOB is shown in Scheme 2. The reaction was carried out in a solvent of acetone in a 100 mL three-neck glass flask equipped with stirrer, thermometer and condenser. A brief description of the procedure follows: 8.8 g of 4-bromomethyl benzophenone was dissolved in 35 mL acetone, and then 10.8 g of octadecyl dimethyl amine was added dropwise. The reaction solution was stirred for 8 h at 55°C. The stirred mixture was cooled to filtration, and washed with acetone and drying under vacuo at room temperature. Then, the crude product was recrystallized using acetone as the solvent. After drying at room temperature under vacuo conditions, the purified BDOB (14.6 g; m.p. 226.5-227.4°C) was obtained as white crystals. FTIR (KBr), v/cm^{-1}: 2934, 2842, 1666, 1454, 932, 715. ^{1}H-NMR ($CDCl_3$, ppm): 0.89 (t, 3H); 1.25 (s, 32H); 3.5 (s, 8H); 5.3 (s, 2H); 7.3-7.9 (m, 9H).

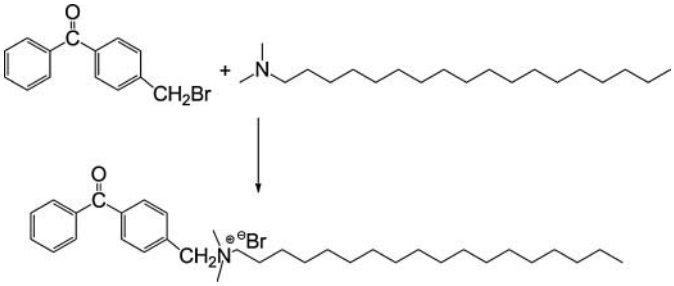

Sch. 2. Scheme for the synthesis of the photo-initiator BDOB.

2.3 Preparation of BDOB-modified MMT (OMMT)

BDOB-modified MMT was prepared by the following procedures: 5 g of Na-MMT was suspended in 1 L of a distilled water-methanol solution [5/6 = water/methanol(v/v)], and the mixture was stirred overnight. To this stirred clay suspension, a solution of BDOB (2.1 g of BDOB in 60 mL of water-methanol solution [5/6 = water/methanol (v/v)]) was added dropwise. After the solution was stirred for another 10 h at room temperature, the precipitate was filtered and washed repeatedly with a water-methanol solution [water/methanol = 5/6 (v/v)] until no bromide ion could be detected by an acidic aqueous $AgNO_3$ solution and no BDOB was detected by high-performance liquid chromatography (HPLC). After drying at 40°C under vacuo overnight, this organically modified clay was ground into powder form with a particle size of less than 45 μm.

2.4 Preparation of the UV-cured EA/MMT Nanocomposites

UV-cured EA/MMT nanocomposites were prepared by the following procedures. The reactive diluent TPGDA was added into bisphenol A epoxy diacrylate (EA), and this mixture was stirred for 2 h to disperse the resin. The OMMT was used as the only photo-initiator in the UV-curable formulation, and the clay loadings in these systems varied from 1 to 5 wt%. A comparative experiment was performed. In the comparative experiment, the loadings of pristine clay were varied from 0 to 3%, meanwhile 1% BDOB was added as the photo-initiator. To avoid premature polymerization caused by the light, the samples were wrapped by aluminum foil. After being homogenized using high speed emulsifier at 30°C for 2 h and ultra-sonized for 8 h, the sample was degassed under vacuo to remove the entrapped air. The resins were injected into a 2 mm thick organic glass gasket (length 150 × width 50 (mm)), sandwiched between two glass slides and PET films to allow easy removal of the samples. Samples were exposed to the UV radiation from a high pressure mercury lamp (output power of 600 w/cm^2). The incident light intensity at the sample position was measured by radiometry to be 400 w/cm^2. A shutter was used to allow accurate control of the exposure time of the sample to the light. Samples were exposed to the UV lamp for a total time of 2 min (1 min on each side) at ambient temperature.

2.5 Characterization

Fourier transform infrared spectrometer (FTIR) was performed on a WQF-200 instrument (Rayleigh, China) using conventional KBr pellets. Proton nuclear magnetic resonance (^{1}H-NMR) spectra were collected by an Inova 400 spectrometer (Palo Alto, CA) using $CDCl_3$ as solvent. High-performance liquid chromatography (HPLC, Alltech, ELSD 800) was used to detect the BDOB, and the mobile phase was a methanol-water solution [8/2 = methanol/water (v/v)] with flow velocity of 1 mL/min. Thermogravimetric analysis (TGA) was performed on a Netzsch STA409PC instrument (Netzsch, Germany) under a flowing nitrogen atmosphere from 30 to 700°C at a scan rate of 10°C/min. Differential scanning calorimetry (DSC) was performed on a TA Instruments Q 20 series calorimeter (TA, USA). Samples were subjected to a heat, cool, heat cycle from −20 to 200°C at a ramp rate of 10°C/min. T_g were determined as the mid-point of the inflection from the 2nd heat cycle, and the reported values were the averages of three determinations. X-ray diffraction (XRD) patterns were collected from 0.5 to 10° and a scan time of 10 s/step using a Bruker D8 instrument (Bruker, Germany) using a step size of 0.1°. Transmission electron microscopy (TEM) images of the composites were obtained at 80 kV with a TEM-1230 (JEOL, Japan). The mechanical properties were conducted according to ASTM D638 by using WDW 3020 testing machine with a computerized system (WDW, China), and the reported values were the averages of five determinations.

3 Results and Discussion

3.1 Structure and Thermal Stability of OMMT

3.1.1. *FTIR spectrum of Na-MMT, BDOB and OMMT*

Figure 1 shows the typical FTIR spectrum of pristine MMT, BDOB, and OMMT, and characteristic peaks of the BDOB and the MMT are summarized in Table 1. Besides the typical bands in the pristine MMT, some new absorbance bands are present in the FTIR spectrum of OMMT. The Si-O stretching band, observed at 1046 cm^{-1} in the pristine clay (Fig. 1(a)), can also be observed in the

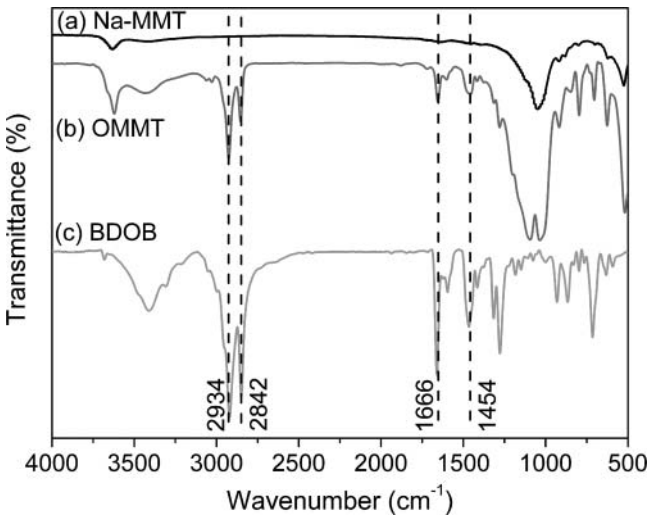

Fig. 1. FTIR spectra obtained from: (a) Na-MMT; (b) OMMT; (c) BDOB.

Table 1. Characteristic FTIR peaks for BDOB and Na-MMT

	Group	*Wavenumber (cm^{-1})*
	$\upsilon(CH_2$, as)	2934
	$\upsilon(CH_2$, s)	2842
BDOB	υ(C=O)	1666
	$\delta(CH_3$, as) $\delta(CH_2$, s)	1454
	δ(=CH) (out-of-plane)	932
	ρ(CH)	715
Na-MMT	υ(OH)	3635
	υ(Si-O-Si, as)	1046
	δ(OH) (out-of-plane)	932
	υ(Al-O-Si)	541

OMMT (Fig. 1(b)). The band at 1666 cm^{-1} in OMMT is attributed to the C=O stretch of carbonyl groups. Evidence of aluminum ion among layers of MMT exchanging with the surfactant can be clearly seen by the presence of CH_2 stretching peaks at 2934 and 2842 cm^{-1} and CH_2 bending peaks at 1454 cm^{-1} in the FTIR spectrum of OMMT (Fig. 1(b)). The above evidence indicates that OMMT has been obtained.

3.1.2. *TGA Characterization of Na-MMT and OMMT*

Figure 2 shows the thermal degradation behaviors of the OMMT and Na-MMT. It is obvious that there are two degradation steps at 203 and 338°C for BDOB. The initial degradation, occurred at 203°C, is attributed to a Hoffman degradation mechanism of the quaternary ammonium salts (21). For OMMT, the initial degradation temperature is 250°C, which indicates higher thermal stability compared with BDOB.

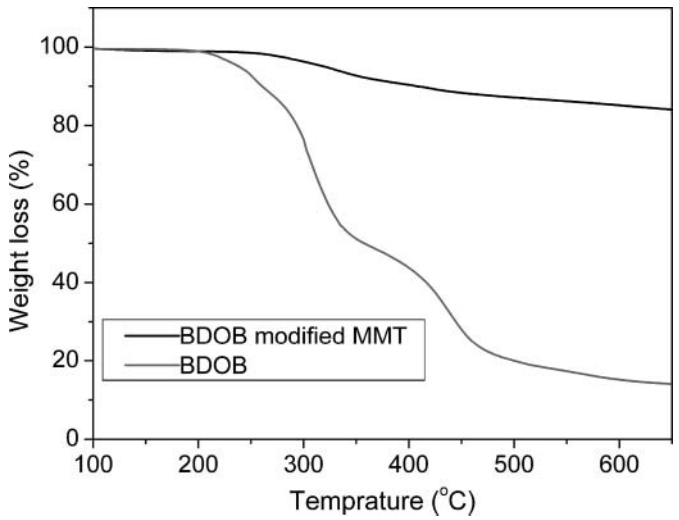

Fig. 2. TGA traces obtained for BDOB and BDOB modified MMT.

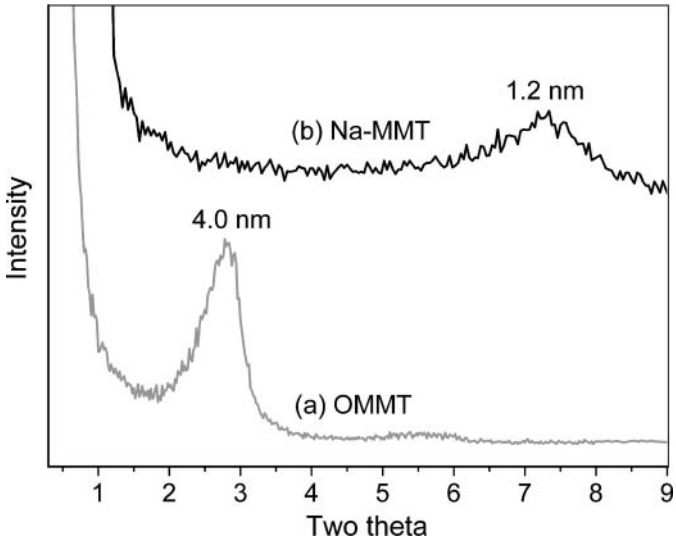

Fig. 3. XRD traces obtained from: (a) OMMT; (b) Na-MMT.

3.1.3. *XRD Results of Na-MMT and OMMT*

The XRD diffraction patterns are shown in Figure 3. The spacing is calculated on the basis of Brag's law [$d = \lambda/(2 \sin \theta)$] at the peak position.The peak at 7.0° corresponds to a d-spacing of 1.2 nm for pristine clay, and the peak at 2.8° corresponds to a d-spacing of 4.0 nm for OMMT. The increase of the d-spacing (2.8 nm) is due to the incorporation of functionalized surfactant BDOB. This result further confirms that an intercalated structure of OMMT has been obtained.

3.2 Cure Time of UV-cured Intra-gallery Polymerization

In general, cure refers to the crosslinking of a polymer to produce a three dimensional network, and the observed phenomenon include a change in the refractive index and in tackiness in the cure process. In this experiment, the time for the formation of a tack-free film has been taken as the cure time for a complete conversion. The cure time for both pristine clay/EA and OMMT/EA systems have been listed in Table 2. These experimental data have indicated that the cure time is not significantly affected by the presence of clay in the pristine clay/BDOB system (14, 16). However, the situation for the OMMT system is different, because the anchored photo-initiator acts as the only initiator in the cure process. Even though more a calculated initiator has been used, it takes longer time to cure completely. The reasonable account is that the photo-initiator is anchored in the gallery of the clay, and the intensity of the UV radiation acting on the photo-initiator is reduced, which leads to a slower cure process of the acrylate. At the same time, a reduced cure time is observed when the amount of OMMT is increased in the OMMT system.

Table 2. Cure time of UV-cured composites for complete conversion

	EA/MMT	*EA/MMT*	*EA/OMMT*	*EA/OMMT*	*EA/OMMT*
Clay Weight (%)	0	3	1	3	5
Initiator Weight (%)	1	1	0.24	0.72	1.2
Cure time (s)	13	13	21	16	14

3.3 The Effect of OMMT Content on Photopolymerization

Figure 4 illustrates typical FTIR spectra of EA/OMMT UV-cured nanocomposites with 3% OMMT during UV curing. The absorption peak for C=C of the acrylate occurs near 1635 cm^{-1} and that for C=O of the acrylate at 1730 cm^{-1}. As the curing reaction proceeds, the concentration of C=C groups is decreased, while that of the C=O groups remains almost unchanged. As a result, the area under peak of C=C can be used to quantitate the change in the concentration of C=C using the C=O peak as a reference or internal standard (22). The ratio of the area under peak of C=C to that under peak C=O was used to measure the % conversion of the EA to network at room temperature (Equation 1):

$$X(t) = (1 - R_t/R_0) \times 100 \quad (1)$$

Where $X(t)$represents % conversion of EA to polymer at time t, R_t is the ratio of peak of C=C area to peak of C=O area at time $t$and R_0 denotes the ratio of peak of C=C area to peak of C=O area at time 0.

The spectra were quantified using this method to calculate the percentage of prepolymer conversion. EA does not achieve complete conversion at room temperature regardless of the apparent formation of the solid film. Relative to the higher OMMT concentration, 1% OMMT appears to cause almost the same initial curing rate yet yields a lower percentage conversion of 55.7% compared to 61.8% conversion for the 5% OMMT-containing film (Fig. 5).

3.4 XRD and TEM Results of EA/OMMT UV-cured Nanocomposites

Figure 6 shows the XRD diffraction patterns of OMMT and EA/OMMT nanocomposites at different levels of OMMT. The XRD peak of OMMT appears at 2.8°, which corresponds to d-spacing of 4.0 nm due to the intercalation of photo-initiator molecules in the clay galleries. There is no characteristic peak from 1 to 10° for the OMMT UV-cured nanocomposite. This result suggests that the clay platelets should be exfoliated or completely disordered. However, the absence of an XRD peak of nanocomposite containing 1 to 5 wt% clay in EA/OMMT does not necessarily mean exfoliation, as the observed absence of scattering could be attributed to geometry effects or lack of sensitivity at the low level of clay loading.

Compared with XRD diffraction patterns, TEM can get more direct structure characterization of the nanocomposites. Figure 7 shows typical TEM images of samples. The low magnification image (Fig. 7(a)) indicates that MMT is well dispersed in the UV-cured polymer. At high magnification, the TEM image (Fig. 7(b)) reveals thin isolated clay layers and parallel clay layers on the edge

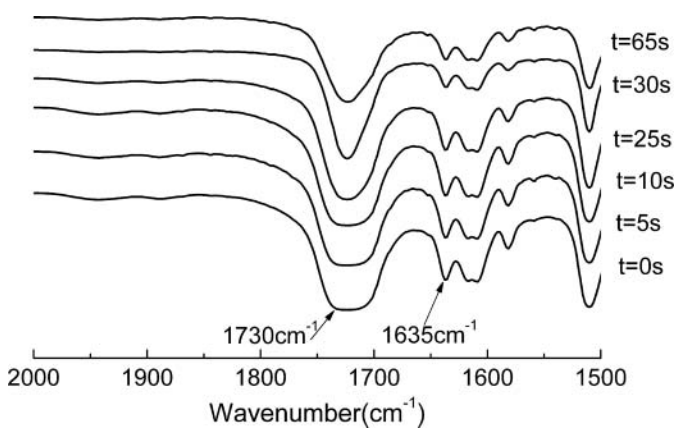

Fig. 4. The FTIR of UV-cured OMMT/EA nanocomposites at different irradiation time (3% OMMT).

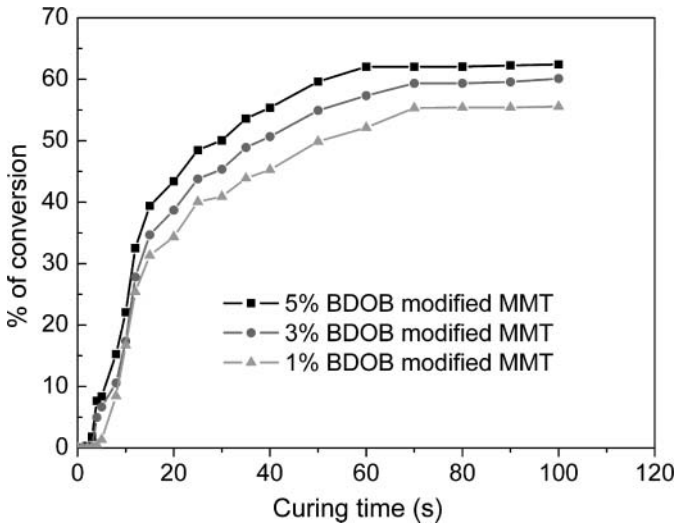

Fig. 5. The effect of OMMT content on photopolymerization.

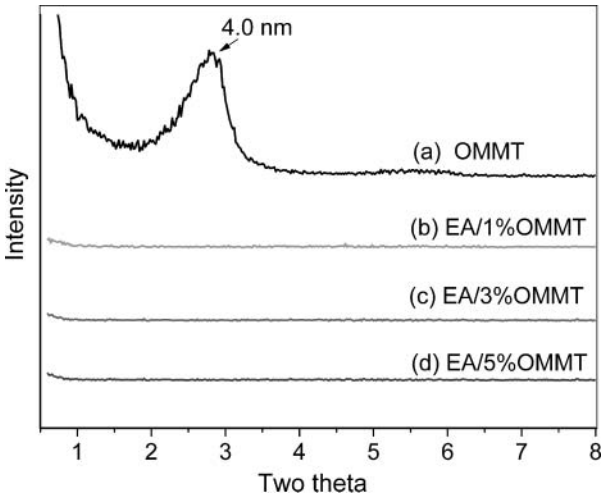

Fig. 6. XRD traces obtained form (a) OMMT and EA/OMMT UV-cured nanocomposites at OMMT loading of (b) 1 wt%, (c) 3 wt% and (d) 5 wt%.

of the clay particles, which indicates that a mixture of partially exfoliated and intercalated structures presented in the nanocomposites.

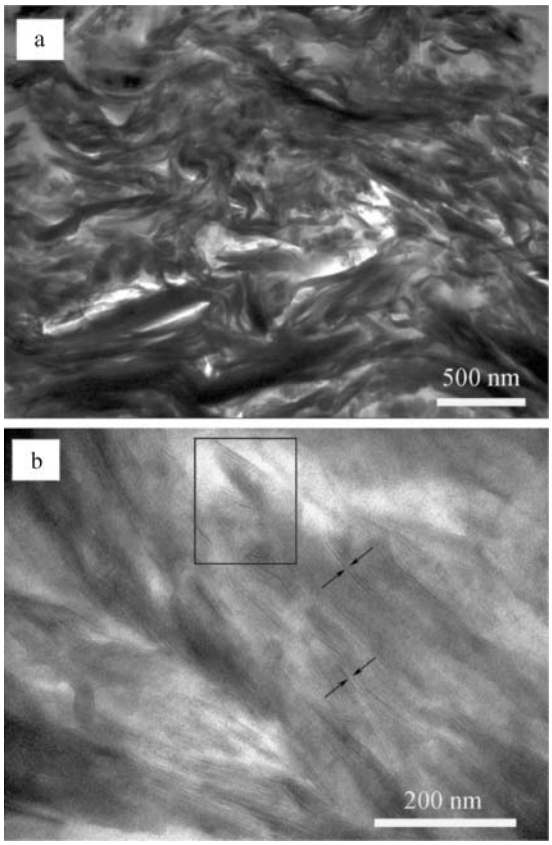

Fig. 7. TEM images of UV-cured OMMT/EA nanocomposites at clay loading of 3 wt%: (a) low magnification (b) high magnification.

Table 3. The decomposition of UV-cured EA/OMMT composites

Organic modified clay	$T_{10\%}$ (°C)	$T_{50\%}$ (°C)	*Char (%)*
Pure EA	304	408	8.8
EA/5%OMMT	345	417	18.7
EA/3%OMMT	341	418	13.9
EA/1%OMMT	338	415	15

3.5 Thermal Properties of EA/OMMT UV-cured Nanocomposites

The thermal stability of pure EA and EA/OMMT UV-cured nanocomposites are evaluated by TGA and DSC. The results are presented graphically in Figures 8 and 9, and Table 3. Generally, information obtained from TGA analysis includes: the 10% weight loss temperature ($T_{10\%}$), the measure of the onset degradation; the 50% weight loss temperature ($T_{50\%}$), the midpoint of the degradation process; and the remaining fraction of material at 700°C is denoted as char. The TGA results show that onset degradation temperature of pure EA appeared at 304°C. With an increase of OMMT, the onset degradation temperatures all shift to higher temperature. The onset degradation temperatures of EA/1%OMMT, EA/3%OMMT and EA/5%OMMT have respectively increased about 34, 37 and 41°C, which demonstrates an increase of the thermal stability. Therefore, the nanocomposites possesses higher thermal stability than pure EA due to the strong interaction between OMMT layers and EA. In addition, the polymer is confined in the interlayer and could not move freely, so the degradation process is also changed.

Figure 9 lists T_g of the pure EA and photo-cured nanocomposites which were obtained from DSC experiments. The photo-cured nanocomposites containing

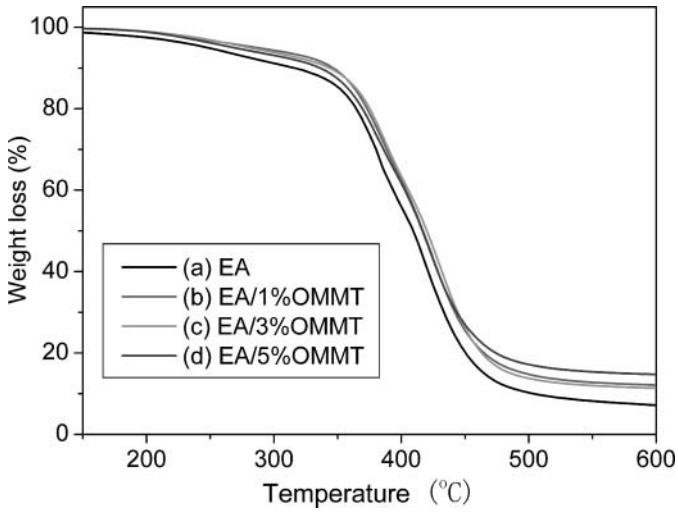

Fig. 8. TGA traces obtained from EA polymer and its nanocomposites.

Table 4. Mechanical properties for the nanocomposites

	Pure EA	EA/1%OMMT	EA/3%OMMT	EA/5%OMMT
Tensile strength (MPa)	26	44	35	34
Tensile modulus (GPa)	1.2	1.8	1.6	1.6
Elongation at break (%)	3.1	4.8	4.6	4.3

BDOB modified MMT have higher T_g than that of the pure EA because of the confinement of the polymer chains between the clay layers limiting segmental motion of the polymer chain (23).

3.6 Mechanical Properties of EA/OMMT UV-cured Nanocomposites

Table 4 shows the effect of MMT content on the tensile strength, tensile modulus and elongation at break. The pure EA has a tensile strength of 26 MPa and tensile modulus of 1.2 GPa. The tensile strength of nanocomposites increases rapidly with increasing OMMT content, from 0 to 1%. When only 1% OMMT is added, the tensile strength of nanocomposites is 44 MPa: an approximate 69% increase in tensile strength is obtained. Therefore, the reinforcement effect may be caused by interactions of the organoclay particles and the EA matrix, that is, hydrophobic interactions between the alkyl chains of organoclay and the EA (24–27). The tensile strength of the nanocomposites, however, decreased for OMMT amounts higher than 1%. The tensile strength of EA/3%OMMT, EA/5%OMMT was 35MPa, 34MPa, respectively, which is higher than that of pure SBS, but less than that of EA/1%OMMT. The decrease in the tensile strength with increasing amount of OMMT from 1 to 5% may be attributable to the slip in the interface between the OMMT particles and the EA matrix. That is, an excess of organoclay particles may prevent the interaction between the organoclay particles and the EA matrix (27). A similar phenomenon is observed in Table 4 for tensile modulus and elongation at break. However, the result is different with our laboratory's previous study (20), that is because they synthesized a bifunctional reactive surfactant to modify montmorillonite (MMT). But, in this paper, we synthesized a novel long chain surfactant, to modify the montmorillonites (MMT).

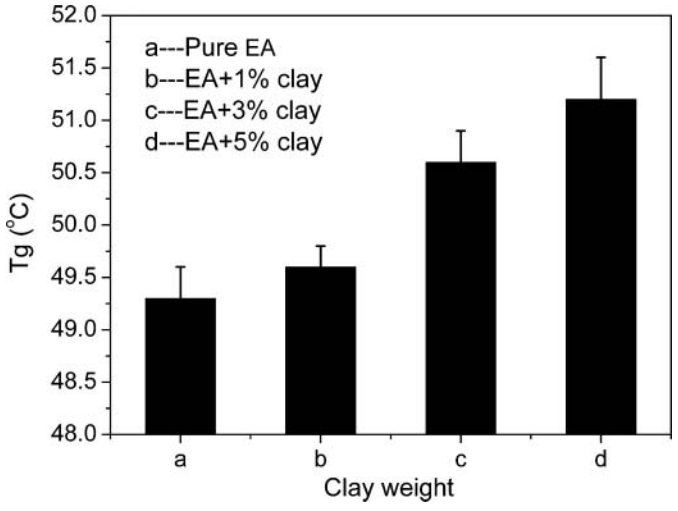

Fig. 9. Effect of clay content on DSC glass transition temperatures (T_g).

4 Conclusions

BDOB, a long chain cationic photo-initiator, has been used to prepare the OMMT and its EA nanocomposites which can be used in the electronic polymer The conversion of the prepolymer was quantified by the FTIR, and the results indicated that the highest conversion was 61.8% with 5 wt% OMMT. The structures of the resulted UV-cured nanocomposites are characterized by XRD and TEM. The results show that MMT is an intercalated structure and disperses well in the polymer. The overall performance of this material suggestes that the current approach with the anchored initiator inside the clay galleries is a promising strategy for the preparation of high performance photopolymer nanocomposites.

Acknowledgments

This research was financially supported by the Hunan Province Science and Technology Program in 2008, China.

References

1. Decker, C. (1996) *Prog. Polym. Sci.*, 21(4), 593–650.
2. Cook, W.D. (1993) *J. Polym. Sci. Part A: Polym. Chem.*, 31, 1053–1067.
3. Andrzejewska, E. (2001) *Prog. Polym. Sci.*, 26(4), 605–665.
4. Vora, R.H. and Goh, S.H. (2006) *Mater. Sci. Eng. B*, 132, 24–33.
5. Su, S.P. and Wilkie, C.A. (2003) *J. Polym. Sci. PartA: Polym. Chem.*, 41, 1124–1135.
6. Wang, N., Zhao, C.L., Shi, Z.X., Shao, Y.W., Li, H.W. and Gao, N. (2009) *Mater. Sci. Eng. B*, 157, 44–47.
7. Araújo, E.M., Mélo, T.J.A., Santana, L.N.L., Neves, G.A., Ferreira, H.C., Lira, H.L., Carvalho, L.H., A'vila Jr., M.M., Pontes, M.K.G. and Araújo, I.S. (2004) *Mater. Sci. Eng. B*, 112, 175–178.
8. Zahouily, K., Benfarhi, S., Bendaikha, T., Baron, J. and Deck, C. (2001) *Proc. Rad. Tech. Europe Conference*, 583.

9. Mousa, A. and Karger-Kocsis J. (2001) *Macromol. Mater. Eng.*, 286, 260–266.
10. Tien, Y.I. and Wei, K.H. (2001) *Polymer*, 42, 3213–3221.
11. Benfarhi, S., Decker, C., Keller, L. and Zahouily, K. (2004) *Eur. Polym. J.*, 40, 493–501.
12. Wang, Z.C., Xua, C.L., Zhao, Y.Q., Zhao, D.D., Wang, Z., Li, H.L. and Lauc, K.-T. (2008) *Mater. Sci. Eng. A*, 490, 481–487.
13. Decker, C., Keller, L., Zahouily, K. and Benfarhi, S. (2005) *Polymer*, 46, 6640–6648.
14. Benfarhi, S., Decker, C., Keller, L. and Zahouily, K. (2003) *Eur. Polym. J.*, 40(3), 493–501.
15. Uhl, F.M., Hinderliter, B.R., Davuluri, P.S., Croll, S.G., Wong, S.C. and Webster, D.C. (2003) *Polym. Prepr.*, 44(2), 247–255.
16. Uhl, F.M., Davuluri, S.P., Wong, S.C. and Webster, D.C. (2004) *Polymer*, 45(18), 6175–6187.
17. Keller, L., Decker, C. Zahouily, K. and Benfarhi, S. (2004) *Polymer*, 45(22), 7437–7447.
18. Yebassa, D., Balakrishnan, S., Feresenbet, E., Raghavan, D. Start, P.R. and Hudson, S.D. (2004) *J. Polym. Sci. PartA: Polym. Chem.*, 42(6), 1310–1321.
19. Wang, Y.Y. and Hsieh, T.-E. (2005) *Chem. Mater.*, 17, 3331–3337.
20. Zang, Y.L., Xu W. J., Liu, G. P., Qiu, D.Y., Su, S.P. (2009) *J. Appl. Polym. Sci.,* 111, 813–818.
21. Shemper, B.S., Morizur, J.F., Alirol, M., Domenech, A., Hulin, V. and Mathias, L.J. (2004) *J. Appl. Polym. Sci.*, 93, 1252–1263.
22. Wang, Z.Y., Bogner, R.H., (1995) *Int. J. Pharm.,* 113(10), 113–122.
23. Ogawa, M. and Kuroda, K. (1997) *Bull. Chem. Soc. Jpn.*, 70, 2593–2618.
24. Mejiritski, A., Sarker, M.A., Wheaton, B. and Neckers, C.D. (1997) *Chem. Mater.*, 9, 1488–1496.
25. Uthirakumar, P., Nahm, K.S., Hahn, Y.B. and Lee, Y.-S. (2004) *Eur. Polym. J.*, 40, 2437–2444.
26. Sue, H.-J., and Gam, K.T. (2004) *Chem. Mater.*, 16, 242–249.
27. Yamaguchi, T., Yamada, E. (2006) *Polym. Int.*, 55, 662–667.